

NUMERICAL SIMULATIONS OF TWO-PHASE FLOWS IN MICRO GAS/LIQUID MIXING SECTIONS

Mahidhar Tatineni* and Xiaolin Zhong†

University of California, Los Angeles, California 90095

Abstract

This paper presents a numerical study of multiphase flows in a micro gas/liquid mixing section. The numerical simulation tool is based on the level set advection equation coupled with incompressible Navier-Stokes equations in both the gas and liquid phases. The numerical scheme is based on a standard staggered Marker and Cell (MAC) grid for discretization. The spatial discretization is carried out by using a fifth order Weighted Essentially Non-Oscillatory (WENO) scheme for the convective terms and a second order discretization for all other terms. The numerical simulation tool is used to study a cross-shaped gas/liquid mixing section which produces monodisperse gas bubbles coflowing with liquids in a micro-channel. The surface tension, liquid flow rates and gas flow rates are varied to study the bubble generation process. A simple theoretical model is also developed to predict the size of the bubbles generated. The numerical results are in good agreement with both the theoretical and experimental results. Further simulations are carried out with a T-shaped mixing section to validate the proposed theoretical model. All numerical simulations are also checked and found to be grid independent.

*Staff Research Associate, Mechanical and Aerospace Engineering Department, Member AIAA.

†Professor, Mechanical and Aerospace Engineering Department, Associate Fellow AIAA, xiaolin@seas.ucla.edu.

Nomenclature

ϕ = Level set function

ρ = Density

μ = Viscosity

g = Acceleration due to gravity

x = Axis aligned with liquid inlets

y = Axis aligned with gas inflow

z = Axis normal to y and x

t = Time

u = Velocity in x direction

v = Velocity in y direction

w = Velocity in z direction

\vec{V} = Velocity vector

∇ = Gradient operator

κ = Interface curvature

σ = Surface tension

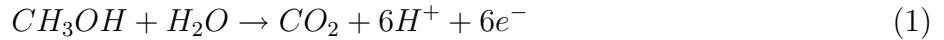
τ = Pseudo time variable

\vec{N} = Normal vector (normal to interface)

1 Introduction

Currently, there is considerable ongoing research on multiphase flows in microfluidic devices. This paper uses numerical simulations as a tool for studying two phase flows in micro gas/liquid mixing sections. The numerical studies in this paper are a part of ongoing research in micro direct methanol fuel cells. Figure 1 shows a schematic of the micro fuel cell considered in the research. There are significant two-phase flow effects on both the anode and cathode side. In the anode

channel the liquid methanol fuel exists with the carbon dioxide bubbles generated by the chemical reaction as follows:



On the cathode side the air drawn in from the ambient exists with the water droplets formed due to the chemical reaction as follows:



Hence, an effective design of the methanol micro fuel cells needs a good understanding of such two-phase flows in micro channels. In order to understand such two-phase flows an experiment was designed by Cubaud et. al. ^[1] which uses an innovative gas/liquid mixing section to produce gas bubbles coflowing with liquid in micro-channels. Previous experimental studies used absolute instabilities in gas microligaments coflowing in a focused liquid stream to produce micro bubbles via a self excited breakup phenomenon^[2, 3]. In this paper, we use a numerical simulation tool based on the level set method to study the above mentioned flows in the mixing section. Some of the results from this numerical study were presented in an earlier AIAA paper ^[4]. In this paper we extend the study with more simulations to ascertain the grid independence of the results and to present a simple theoretical model to predict the sizes of the bubbles generated.

Level set based numerical methods are popular for simulations of multiphase or multimaterial incompressible flows with complex topological changes ^[5, 6, 7, 8, 9]. The approach has also been used in simulating flows in the microscale by using an adaptive level set method ^[10] which can achieve the higher resolution required for microfluidic multiphase studies with minimum additional cost. Sussman and Puckett ^[11] extended and improved the method by coupling the level set method with a volume of fluid method and used it to compute flows in microscale jetting devices. This approach was later extended to a second order coupled level set and volume of fluid method by Sussman ^[12]. The level set methods for two-phase flows can either be based on a continuous surface tension model ^[5, 6] or can be based on the Ghost Fluid Method (GFM) ^[7] which can capture the jump conditions across a contact discontinuity. In the first case the flow properties are considered

to be continuous across the two phase interface and hence the jump conditions are replaced by equivalent continuous terms in the governing equations. In the case of the Ghost Fluid Method, extended to multiphase incompressible flows by Kang et. al. ^[8], the numerical scheme takes into account the jumps in the flow properties and the pressure discontinuities across multiphase interfaces. The pressure Poisson equation was modified to include the pressure jump conditions to effectively solve this problem. In the present numerical study both approaches were used and the results for the mixing section study were found to be good from both approaches. Hence, in the paper most of the simulations are conducted using the simpler continuous model.

In this paper we present studies of two-phase flows in micro mixing section channels. The numerical simulation tool is based on the level set equation coupled with incompressible Navier-Stokes equations for both the fluids. The interface jump conditions are approximated using a continuous surface tension model and flow properties are continuous across the interface. The equations are discretized on a standard MAC grid with velocities on cell walls and the rest of the properties at the cell centers. A fifth order WENO discretization ^[7] is used for the convective terms and a second order discretization is used for the viscous terms. The pressure poisson equation is solved using a multigrid iterative solver. Simulations are considered for both a plus shaped mixing section and a T-shaped mixing section. A simple theoretical model is developed to predict the sizes of the bubbles generated. The numerical results are found to be in good agreement with both the theoretical and experimental results.

2 Governing Equations

2.1 Incompressible N-S Equations for the Two Phases

The basic equations used in the simulations are the incompressible Navier-Stokes equations with the gravitational term and jump conditions at the multimaterial interface. The viscous incom-

pressible equations are:

$$\frac{\partial \rho}{\partial t} + \vec{V} \cdot \nabla \rho = 0 \quad (3)$$

$$\frac{\partial u}{\partial t} + \vec{V} \cdot \nabla u + \frac{p_x}{\rho} = \frac{(2\mu u_x)_x + (\mu(u_x + v_y))_y + (\mu(u_z + w_x))_z}{\rho} \quad (4)$$

$$\frac{\partial v}{\partial t} + \vec{V} \cdot \nabla v + \frac{p_y}{\rho} = \frac{(\mu(u_y + v_x))_x + (2\mu v_y)_y + (\mu(v_z + w_y))_z}{\rho} + g \quad (5)$$

$$\frac{\partial w}{\partial t} + \vec{V} \cdot \nabla w + \frac{p_z}{\rho} = \frac{(\mu(w_x + u_z))_x + (\mu(v_z + w_y))_y + (2\mu w_z)_z}{\rho} \quad (6)$$

where t is the time, (x, y, z) are the spatial coordinates, ρ is the density, $\vec{V} = \langle u, v, w \rangle$ is the velocity field, p is the pressure, μ is the viscosity, and g is the gravity. The viscosity and density parameters are different in the two fluids. The velocity is continuous across the multiphase interface. However, when calculating the viscous terms and solving the pressure poisson solver the jump conditions across the interface need to be calculated. The equations for the jump conditions were derived by Kang et. al. ^[8] as follows:

$$\left[\frac{p_x}{\rho} \right] = \left[\frac{(2\mu u_x)_x + (\mu(u_x + v_y))_y + (\mu(u_z + w_x))_z}{\rho} \right] \quad (7)$$

$$\left[\frac{p_y}{\rho} \right] = \left[\frac{(\mu(u_y + v_x))_x + (2\mu v_y)_y + (\mu(v_z + w_y))_z}{\rho} \right] \quad (8)$$

$$\left[\frac{p_z}{\rho} \right] = \left[\frac{(\mu(w_x + u_z))_x + (\mu(v_z + w_y))_y + (2\mu w_z)_z}{\rho} \right] \quad (9)$$

$$[p] - [\mu](\nabla u \cdot \vec{N}, \nabla v \cdot \vec{N}, \nabla w \cdot \vec{N}) \cdot \vec{N} = \sigma \kappa \quad (10)$$

where σ is the surface tension, and κ is the curvature of the interface. The interface is tracked using the level set equation:

$$\frac{\partial \phi}{\partial t} + \vec{V} \cdot \nabla \phi = 0 \quad (11)$$

where $\phi = 0$ represents the interface location. To keep the values of ϕ close to that of a signed distance function the level set function is reinitialized after every time step using iterations in a pseudo time variable:

$$\frac{\partial \phi}{\partial \tau} + S(\phi_o)(|\nabla \phi| - 1) = 0 \quad (12)$$

The level set function is used to compute the normal vector and the interface curvature as follows:

$$\vec{N} = \frac{\nabla\phi}{|\nabla\phi|} \quad (13)$$

$$\kappa = -\nabla \cdot \vec{N} \quad (14)$$

2.2 Continuous Form

In this paper we mainly use the continuous form of the governing equations without the jump conditions^[5, 13]. In the continuous case the viscosity and density are expressed as functions of the level set function as follows:

$$\mu(\phi) = \mu^- + (\mu^+ - \mu^-)H(\phi) \quad (15)$$

$$\rho(\phi) = \rho^- + (\rho^+ - \rho^-)H(\phi) \quad (16)$$

where $H(\phi)$ is a Heaviside function based on ϕ defined as follows:

$$H(\phi) = \begin{cases} 0 & \phi < -\epsilon \\ \frac{1}{2} + \frac{\phi}{2\epsilon} + \frac{1}{2\pi} \sin\left(\frac{\pi\phi}{\epsilon}\right) & -\epsilon \leq \phi \leq \epsilon \\ 1 & \phi > \epsilon \end{cases} \quad (17)$$

and μ^-, ρ^- represent the fluid where $\phi \leq 0$ and μ^+, ρ^+ represent the fluid where $\phi > 0$. Using the continuous surface force model the pressure is continuous and the remaining jump conditions can be modeled by adding a term of the form

$$\frac{\delta\sigma\kappa\vec{N}}{\rho} \quad (18)$$

to the right hand side of the momentum equations. Note that now the delta function is also smeared out and calculated by taking a derivative of the above Heaviside function.

3 Numerical Method

The discretization of the above equations is performed using a standard MAC grid. The velocities exist at the appropriate cell walls and the pressure, density, viscosity and level set function are

defined at the cell center. The incompressible solver is based on a projection method and the time advancement is carried out using a 3rd order TVD Runge-Kutta method. The convective terms are discretized using a 5th order WENO scheme following the approach of Fedkiw et. al. [7]. For the viscous terms both the continuous delta function approach and the jump conditions approach is used based on the work of Kang et. al. [8]. In the projection method the pressure is solved using the variable coefficient Poisson equations developed in [7]. The resulting poisson equation is solved using a multigrid Gauss-Seidel iterative method.

The numerical procedure has been modified to consider slipping and dynamic contact lines using models. However, in this paper all the simulations assume no contact of the 2-phase boundary with the walls of the microchannels. This is a reasonable assumption for the current study since the experimental cases we compared the results with showed no dewetting and the bubbles were lubricated by a thin liquid film and there were no contact lines.

4 Results

The numerical code used in the simulations was validated by considering the test case of a rising air bubble in water used by Kang et. al. [8] with various grid sizes and the results were presented in an earlier AIAA paper [4]. The validated code was then used to compute the 2-phase flows in the gas/liquid mixing section studied experimentally by Cubaud et. al.[1]. In the experiment there is gas flowing through a microchannel. The liquid is introduced from two sides of the microchannel (forming a cross like section) to pinch the gas flow and form bubbles. In the experiment the gas and liquid flow rates are changed and their effects on the bubbles are studied by high speed camera photos. A simple theoretical model is also proposed to predict the sizes of the bubble generated. The numerical results are compared with both the theoretical prediction and the experimental results.

4.1 Grid Resolution Study Using 2-D Simulations

The resolution requirements for accurately predicting the mixing section flows were ascertained by computing a 2-D test case with a gas velocity of $0.1m/s$ and a liquid crossflow velocity of $0.5m/s$ in a $100\mu m$ by $500\mu m$ channel was computed with grid sizes of 33×161 , 65×321 , 129×641 . For the initial conditions, the channel was assumed to be completely filled with liquid except for a small gas bubble at the entrance. As the simulation progresses more gas enters at the entrance and grows this gas region which is subsequently pinched off by the liquid entering from the side walls to form bubbles. The velocity profile for the gas and liquid inlets is assumed to be parabolic. At the side walls the velocity at the wall is assumed to be zero everywhere except for the area which the liquid enters the domain. Figure 2 shows the development of the gas bubble and the subsequent pinching off due to the crossflow for the three grid sizes. Clearly, the two finer grids are in very good agreement with regards to the bubble size and development rate. The quantitative comparisons for the bubble size and frequency are presented in Table 1. The coarsest grid leads to a difference of 7.08% in bubble size with respect to the finest grid. However, the frequency of the bubble shedding agrees within 1% even with the coarse grid. With the double grid (65×321) case the errors in both frequency and bubble size are less than 0.1%. Hence, the numerical simulations show good convergence with increasing grid sizes. The two dimensional grid independence study is used to determine the appropriate number of grid points for an accurate computation of the flows in the 3-D gas/liquid mixing section.

4.2 Simulations of Flows in Gas/Liquid Mixing Section

After completing the validation and grid independence studies the two phase numerical simulation code is used to study formation of the air bubbles by the break up of a air stream in a microchannel by a crossflow of water from the sides of the microchannel. First, 2-D simulations were carried out to investigate the ability of the code to predict the growth of the gas interface and the pinching process to produce micro bubbles. In addition, the surface tension coefficient was varied

to investigate its effect on the size of the bubbles produced. Finally, full 3-D simulations are conducted for various gas and liquid flow rates and the results are compared with the experimental results of Cubaud et. al.^[1]. The mixing section is considered with liquid flow from two sides (symmetric and plus shaped) or from one side (T-shaped).

2-D Simulation Results for Plus Shaped Section

The 2-D simulations were used in the grid independence study detailed above. In addition, we also used the 2-D simulations to study the effect of varying the surface tension on the bubble sizes and frequencies. The test cases considered air flow in a channel with water crossflow. The surface tension was changed as $\sigma = 0.0728kg/s^2$, $\sigma = 0.01456kg/s^2$, and $\sigma = 0.1456kg/s^2$. The densities and viscosities were kept the same as the air and water values. Figure 3 shows a sequence of plots of the air-water interface, with the pressure contours, to show the pinching process and the formation of the bubble. Figure 4 shows the pinching process for the lower surface tension case. The bubble formed in this case is much smaller than the previous case. When the surface tension is increased, the bubble formed is longer as shown in Fig. 5. Hence, the surface tension is one of the controlling factors in the size of the bubble formed. The results from the 2-D simulations are also tabulated in Table 2 which shows the length of the bubbles formed in each case.

3-D Simulation Results for Plus Shaped Section

The 3-D simulations were conducted for various gas and liquid flow rates to evaluate the bubble sizes and frequencies. Figure 6 shows a schematic of the simulation domain. The inlet velocity profiles were considered to be bi-quadratic. All the simulations are in the low Bond number ($Bo \ll 1$) and low Capillary number ($Ca \ll 1$) regime. The gas Reynolds number is in the range $Re = 1 - 5$, and the liquid Reynolds number is in the range $Re = 20 - 80$. In all the simulations the cross-section is $100\mu m \times 100\mu m$.

From the experimental results one of the important controlling parameter was found to be the homogeneous liquid fraction $\alpha_L = \frac{Q_L}{Q_L+Q_G}$. The numerical simulations were conducted for

homogeneous liquid fractions of 0.5, 0.67, and 0.8. The results were then compared with the experimental results. Figure 7 shows a sequence of plots corresponding to various instants in time, for the $\alpha_L = 0.5$ case. The gas-liquid interface is plotted in the figures. The elongation of the interface and the subsequent pinching due to the liquid crossflow can be clearly seen. The size of the bubble pinched off is about 1.9 times the channel width. The flowfield details can be understood by looking at the instantaneous velocity contours. Figure 8 shows the u velocity contours for a XY cross-section, superposed with the interface location. The liquid flow from the sides is clearly seen. This flow from the two sides squeezes the gas flow and eventually pinches it to form the bubbles. The v velocity contours are shown in Fig. 9. From the figure it is evident that the flow is faster in the section of the bubble which is is squeezed in. Above the bubble the flow returns to a channel flow profile very rapidly. This is also seen in the YZ cross-section plots seen in Fig. 10. Figure 11 shows the w contours in the YZ plane superposed with the interface location. In this case we can see that there is no direct squeezing of the bubble by the liquid (in this plane). The bubble initially almost touches the walls and then thins out because of the flow in the Y direction.

Figure 12 shows pinching process for a higher homogeneous liquid fraction of 0.67. The bubble size is now reduced since the faster liquid velocity results in a quicker pinching of the bubble. When the α_L value is further increased to 0.8 the bubble size is also further reduced. In addition, there is significant deformation of the bubble once it is pinched due to the high liquid velocities pushing it. Hence, based on the above results, we can conclude that the bubble size can be effectively controlled by varying the homogeneous liquid fraction.

Grid Independence Study and Comparisons with Theoretical and Experimental Results

The results from the 3-D simulations are checked for grid independence by using three grid sizes: 32x32, 48x48, and 64x64 for each cross-section (the streamwise grid number is based on the length of the channel used). The bubble sizes obtained are compared in Fig. 14. The results show that the bubble size obtained is grid independent. A theoretical estimate can be obtained for the

bubble sizes by a simple analysis. The estimated time for pinching can be approximated based on the width of the channel (d) and the liquid velocity as follows:

$$T \approx \frac{d/2}{U_L} \quad (19)$$

$$U_L = \frac{Q_L}{2A} \quad (20)$$

$$\Rightarrow T \approx \frac{d A}{Q_L} \quad (21)$$

where Q_L is the total liquid volume flow rate (including both sides). It should be noted that we consider only $d/2$ since the bubble is pinched by the liquid from two sides. The bubble grows at approximately the combined gas and liquid velocity. Hence, a good approximation of the bubble size is as follows:

$$L \approx \frac{Q_L + Q_G}{A} \times T \quad (22)$$

$$\Rightarrow L/d \approx \frac{Q_L + Q_G}{Q_L} = \frac{1}{\alpha_L} \quad (23)$$

From the numerical simulations we have obtained the bubble sizes for various liquid fraction values and compared them with existing experimental results ^[1] as shown in Fig. 14 and the theoretical result derived above. The results show that the numerical simulations are in good agreement with experimental results and the relation developed based on the simple theoretical analysis. The numerical results are found to be within the experimental scatter.

Hence, the 3-D simulations were able to capture the gas/liquid interface development and pinching process observed in the experimental studies. The bubble sizes obtained from the numerical studies are in good agreement with the corresponding experimental results.

3-D Simulations of Flow in T-Shaped Mixing Section

The first set of test cases considered were for a symmetric plus shaped mixing section. In order to study non-symmetric pinching and bubble formation simulations for flow in a T-shaped mixing section are also carried out. This case also serves as a further validation for the theoretical model presented above. The setup of the problem is exactly same as the first case except the

liquid pinching the gas flow is coming in from only one side. Simulations are currently in progress for various flow rates to study the pinching process. Figure 15 shows an instantaneous interface location during the pinching process. The asymmetric development of the bubble can be clearly seen.

Further studies are also in progress for varying channel sizes from macro scales to micro scales in order to ascertain the limits of the simplified theoretical model developed above and to understand the various factors influencing the bubble generation process at different scales. Simulations for longer channels are also in progress to determine the frequencies of bubble generation and to study bubbly flow in microchannels. Figure 16 shows an instantaneous plot from a simulation for a long channel test case. The figure shows the first bubble already detached and the second bubble being formed. Results from a longer time study can give frequency information and help in flow characterization.

5 Conclusions

Two phase flows in micro liquid/gas mixing sections of two different geometries have been simulated using a level set method based numerical simulation tool. Results of both 2-D and 3-D simulations of two-phase flow computations in micro channels have been presented. The results show that the gas and liquid flow rates can be adjusted to produce gas bubbles of varying sizes coflowing with liquid in microchannels. The numerical simulation results for bubble sizes were found to be in good agreement with existing experimental results and a simple theoretical model was developed to predict bubble sizes. The numerical results are also shown to be grid independent using simulations of varying grid resolutions.

6 Acknowledgments

The authors are grateful to Dr. Thomas Cubaud of UCLA for his assistance and for providing the results of his experimental studies. The research presented in the paper is supported by DARPA under the DARPA Micro Power Generation (MPG) program with Dr. Clark T.-C. Nguyen as the program manager.

References

- [1] Cubaud, T. and Ho, C.-M., “Transport of bubbles in square microchannels,” *presented at the Division of Fluid Dynamics 56th Annual Meeting, East Rutherford, New Jersey, Nov 23-25, 2003*.
- [2] Ganan-Calvo, A. M. and Gordillo, J. M., “Perfectly Monodisperse Microbubbling by Capillary Flow Focusing,” *Physical Review Letters*, Vol. 87(27), 2001.
- [3] Gordillo, J. M. and Ganan-Calvo, A. M., “Monodisperse microbubbling: Absolute instabilities in coflowing gas-liquid jets,” *Physics of Fluids*, Vol. 13(12), 2001, pp. 3839–3842.
- [4] Tatineni, M. and Zhong, X., “Numerical Study of Two-Phase Flows in Microchannels Using the Level Set Method,” *AIAA Paper 2004-0929*, 2004.
- [5] Sussman, M., Smereka, P., and Osher, S., “A Level Set Approach for Computing Solutions to Incompressible Two-Phase Flow,” *Journal of Computational Physics*, Vol. 114, 1994, pp. 146–154.
- [6] Chang, Y. C., Hou, T. Y., Merriman, B., and Osher, S., “A Level Set Formulation of Eulerian Interface Capturing Methods for Incompressible Fluid Flows,” *Journal of Computational Physics*, Vol. 124, 1996, pp. 449–464.

- [7] Fedkiw, R., Aslam, T., Merriman, B., and Osher, S., “A Non-Oscillatory Eulerian Approach to Interfaces in Multimaterial Flows (The Ghost Fluid Method),” *Journal of Computational Physics*, Vol. 152, 1999, pp. 457–492.
- [8] Kang, M., Fedkiw, R. P., and Liu, X.-D., “A Boundary Condition Capturing Method for Multiphase Incompressible Flow,” *Journal of Scientific Computing*, Vol. 15, 2000, pp. 323–360.
- [9] Aalburg, C., “Deformation and Breakup of Round Drops and Nonturbulent Liquid Jets in Uniform Crossflows,” *Ph.D. Thesis, Aerospace Engineering and Scientific Computing, University of Michigan*, 2002.
- [10] Sussman, M., Almgren, A. S., Bell, J. B., Colella, P., Howell, L. H., and Welcome, M. L., “An Adaptive Level Set Approach for Incompressible Two-Phase Flows,” *Journal of Computational Physics*, Vol. 148, 1999, pp. 81–124.
- [11] Sussman, M. and Puckett, E. G., “A Coupled Level Set and Volume-of-Fluid Method for Computing 3D and Axisymmetric Incompressible Two-Phase Flows,” *Journal of Computational Physics*, Vol. 162, 2000, pp. 301–337.
- [12] Sussman, M., “A second order coupled level set and volume-of-fluid method for computing growth and collapse of vapor bubbles,” *Journal of Computational Physics*, Vol. 187, 2003, pp. 110–136.
- [13] Brackbill, J. U., Kothe, D. B., and Zemach, C., “A Continuum Method for Modeling Surface Tension,” *Journal of Computational Physics*, Vol. 100, 1992, pp. 335–354.

Table 1: Variation of bubble sizes and frequencies with grid sizes. Gas velocity set at 0.1 m/s, and liquid velocity fixed at 0.5 m/s. The comparisons are made with the finest grid as reference.

Grid Size	Bubble Size	Frequency
33×161	7.08%	1%
65×321	< 0.1%	< 0.1%
129×641	-	-

Table 2: Variation of bubble sizes with surface tension. Gas velocity set at 0.1 m/s, and liquid velocity fixed at 0.5 m/s.

Surface Tension (Kg/s^2)	(Bubble Length)/(Channel Width)
0.0728	1.219
0.01456	0.685
0.1456	1.419

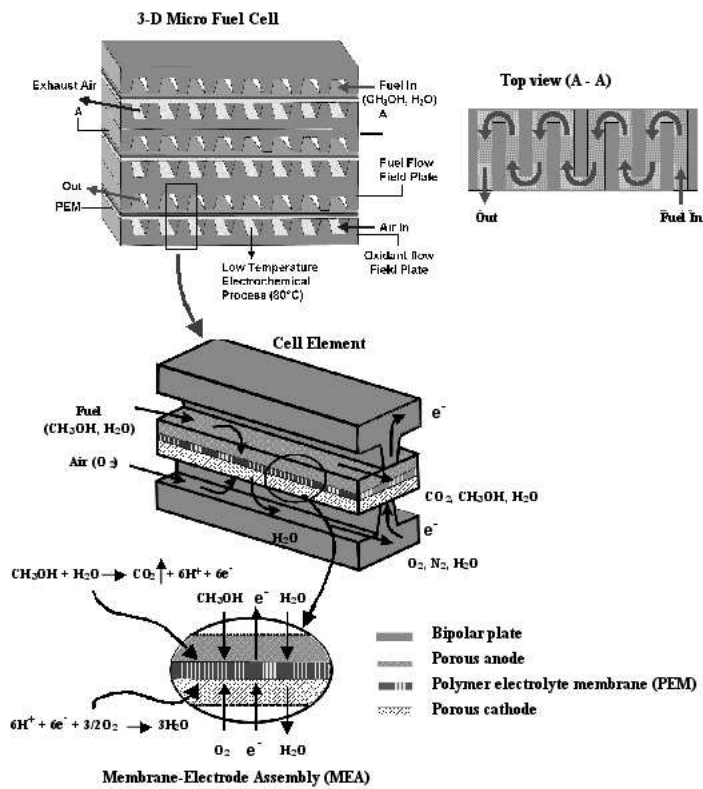


Figure 1: A schematic of a micro direct methanol fuel cell showing the fuel cell structure and the chemical reactions involved.

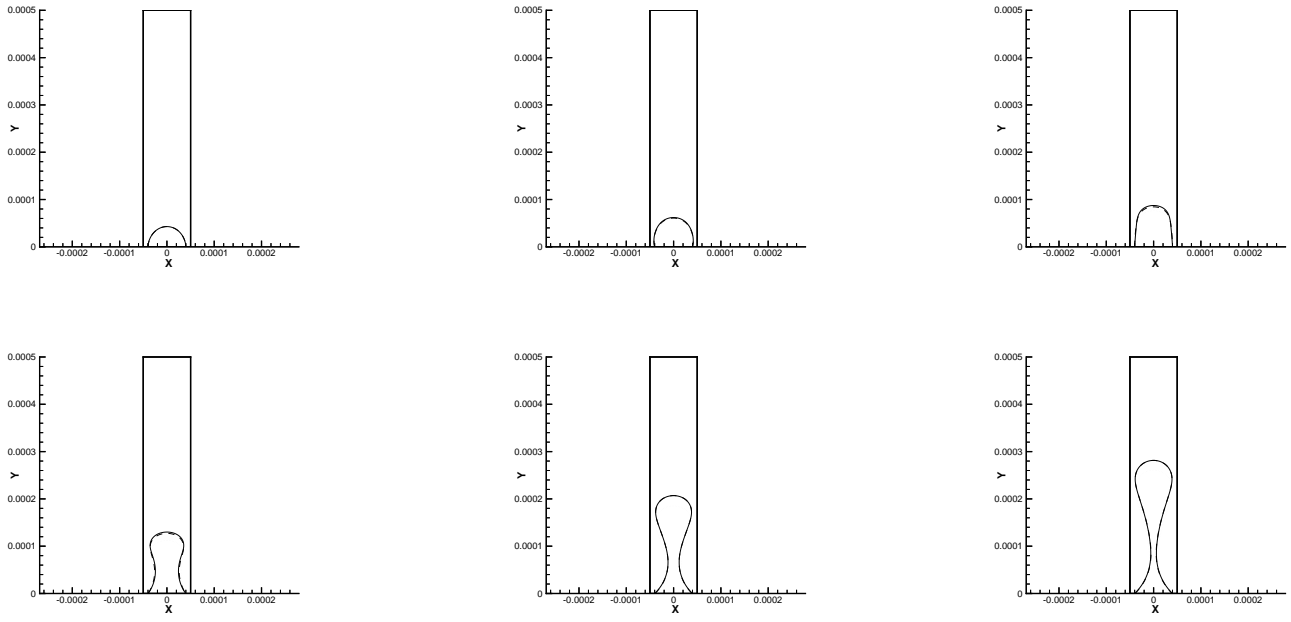


Figure 2: Sequence of figures, each showing pressure contours and phase boundaries, illustrating the formation of bubbles in 2-D microchannel. Computations for air and water as the two fluids and domain size of $100\mu\text{m} \times 500\mu\text{m}$. Simulations performed using 33×161 (dotted) , 65×321 (dashed lines), and 129×641 grids (solid lines) as a part of grid independence study.

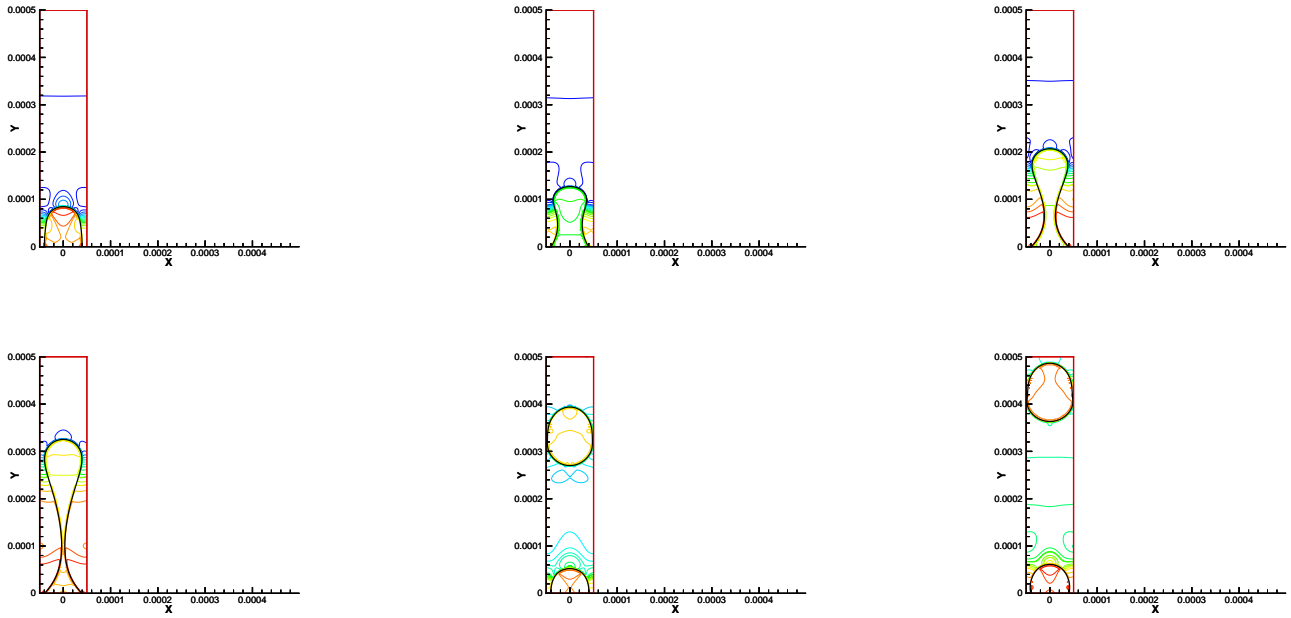


Figure 3: Sequence of figures, each showing pressure contours and phase boundaries, illustrating the formation of bubbles in 2-D microchannel. Air and water considered as the two fluids with surface tension coefficient set as $0.0728\text{kg}/\text{s}^2$.

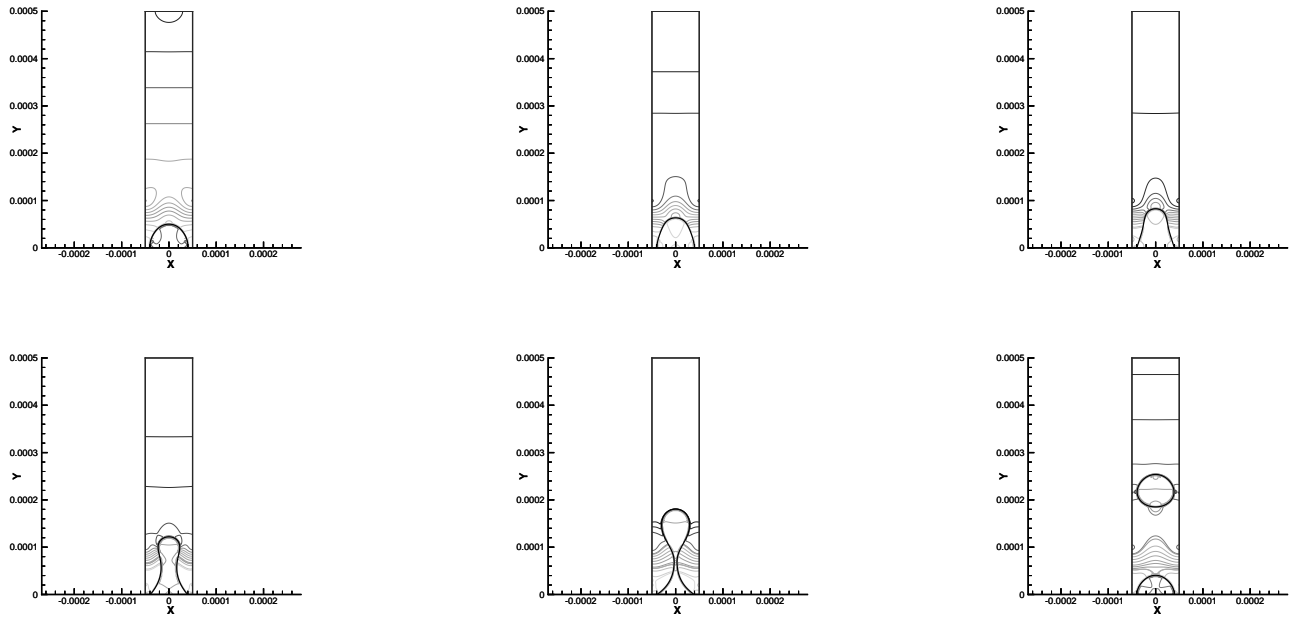


Figure 4: Sequence of figures, each showing pressure contours and phase boundaries, illustrating the formation of bubbles in 2-D microchannel. Test case with decreased surface tension of $0.01456\text{kg}/\text{s}^2$.

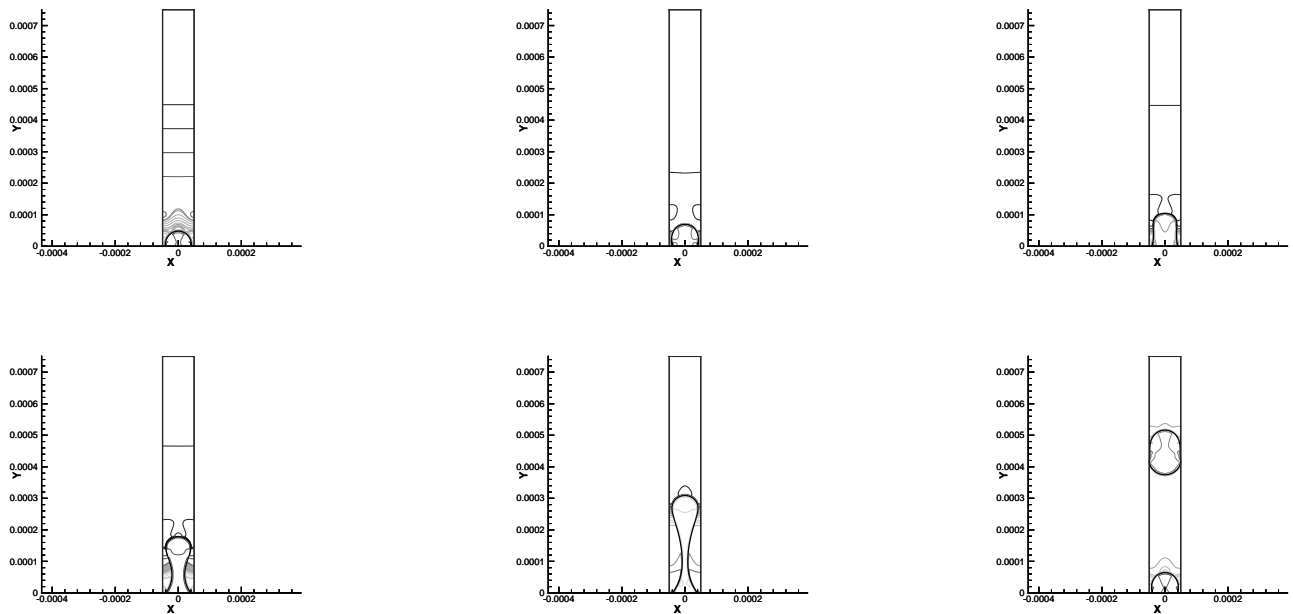


Figure 5: Sequence of figures, each showing pressure contours and phase boundaries, illustrating the formation of bubbles in 2-D microchannel. Test case with increased surface tension of $0.1456\text{kg}/\text{s}^2$.

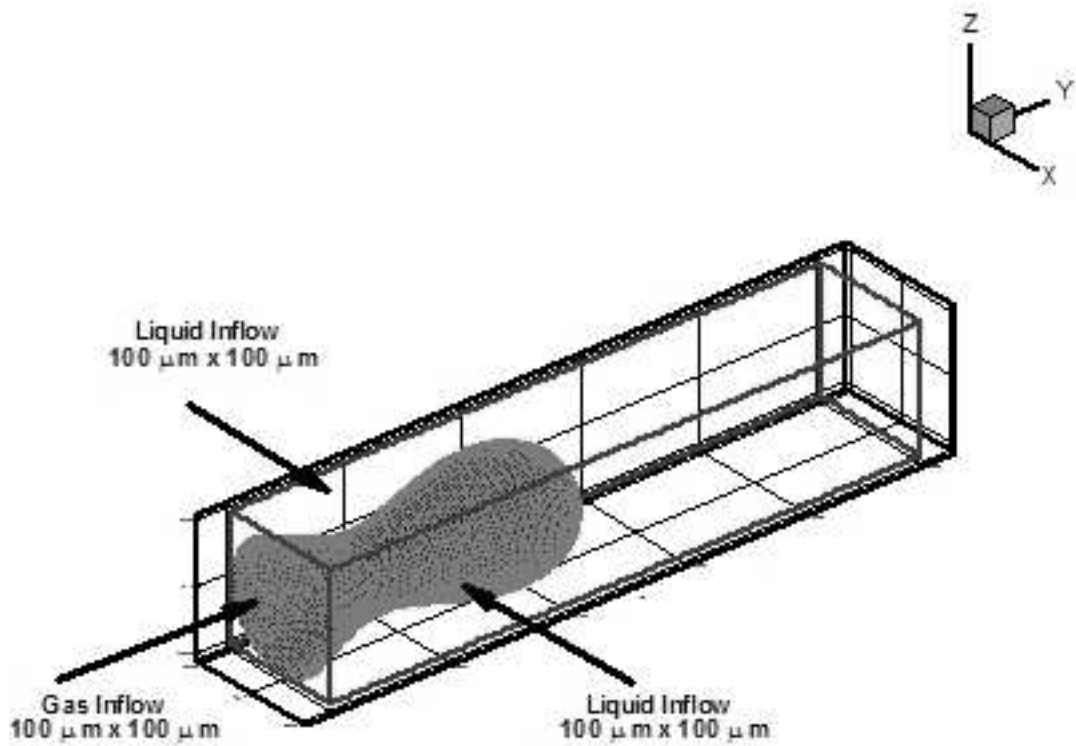


Figure 6: Schematic of the computational domain for 3-D microchannel simulations.

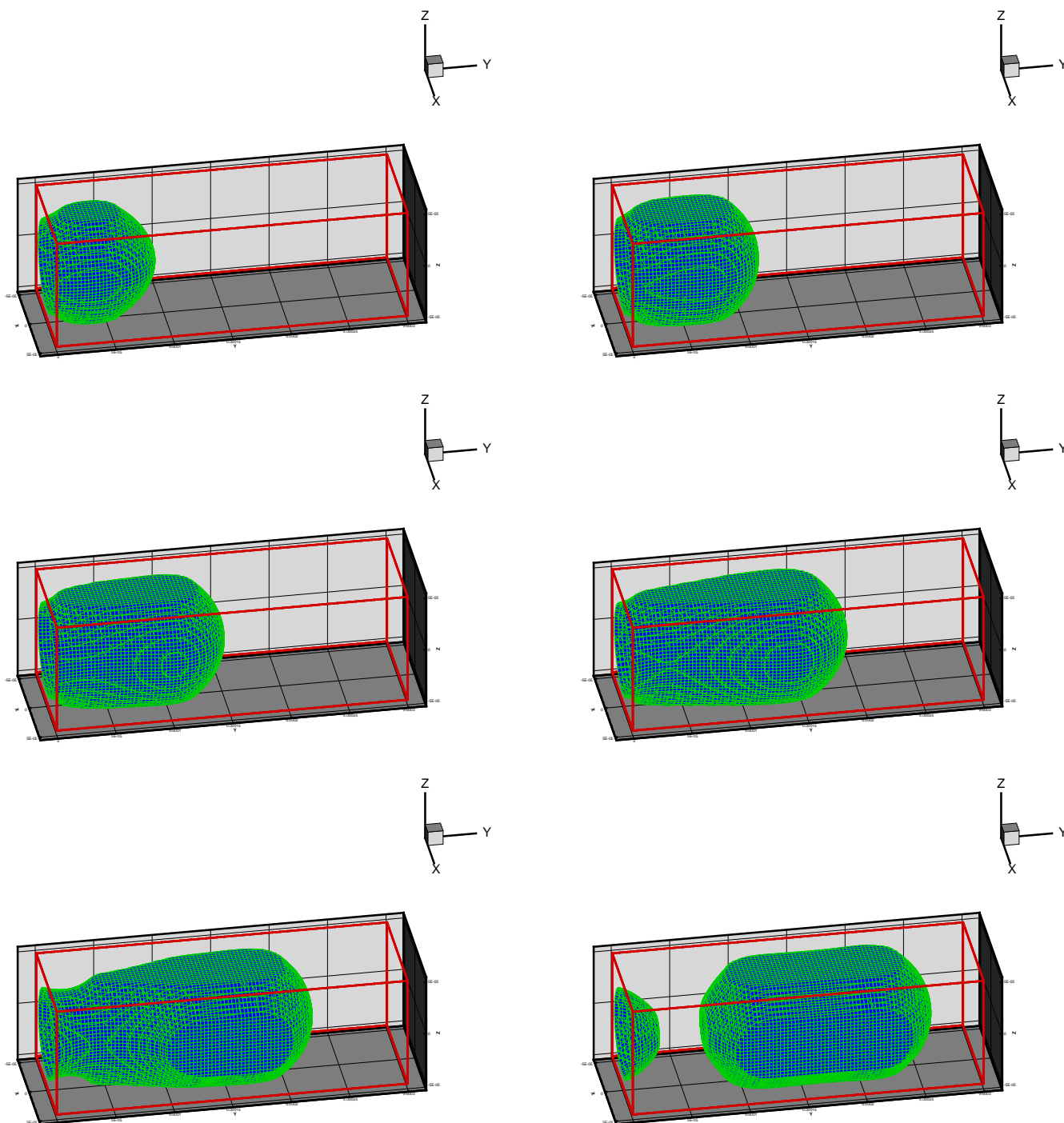


Figure 7: A sequence of figures showing the development and detachment of an air bubble in the crossflow mixing channel. Flow rates correspond to $Q_L/(Q_L + Q_G) = 0.5$.

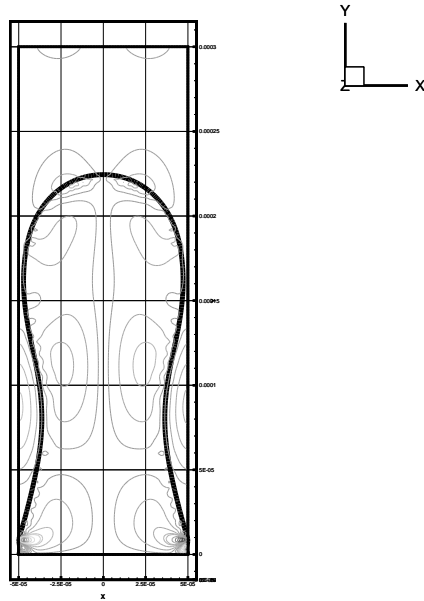


Figure 8: A cross-section (XY plane) of the flowfield showing the interface location and u velocity contours. Results for the $Q_L/(Q_L + Q_G) = 0.5$ case.

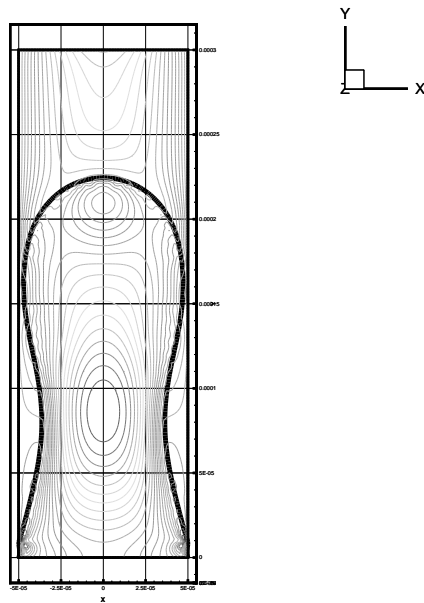


Figure 9: A cross-section (XY plane) of the flowfield showing the interface location and v velocity contours. Results for the $Q_L/(Q_L + Q_G) = 0.5$ case.

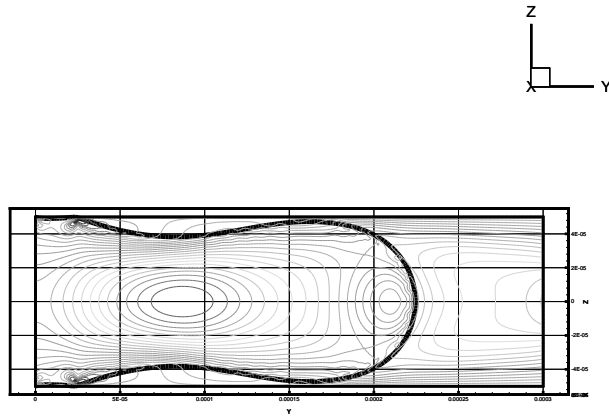


Figure 10: A cross-section YZ plane of the flowfield showing the interface location and v velocity contours. Results for the $Q_L/(Q_L + Q_G) = 0.5$ case.

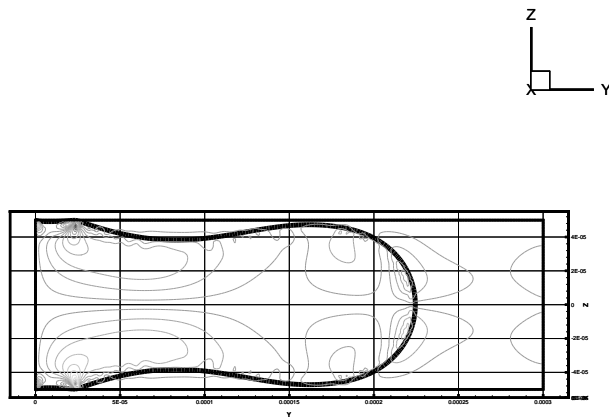


Figure 11: A cross-section YZ plane of the flowfield showing the interface location and w velocity contours. Results for the $Q_L/(Q_L + Q_G) = 0.5$ case.

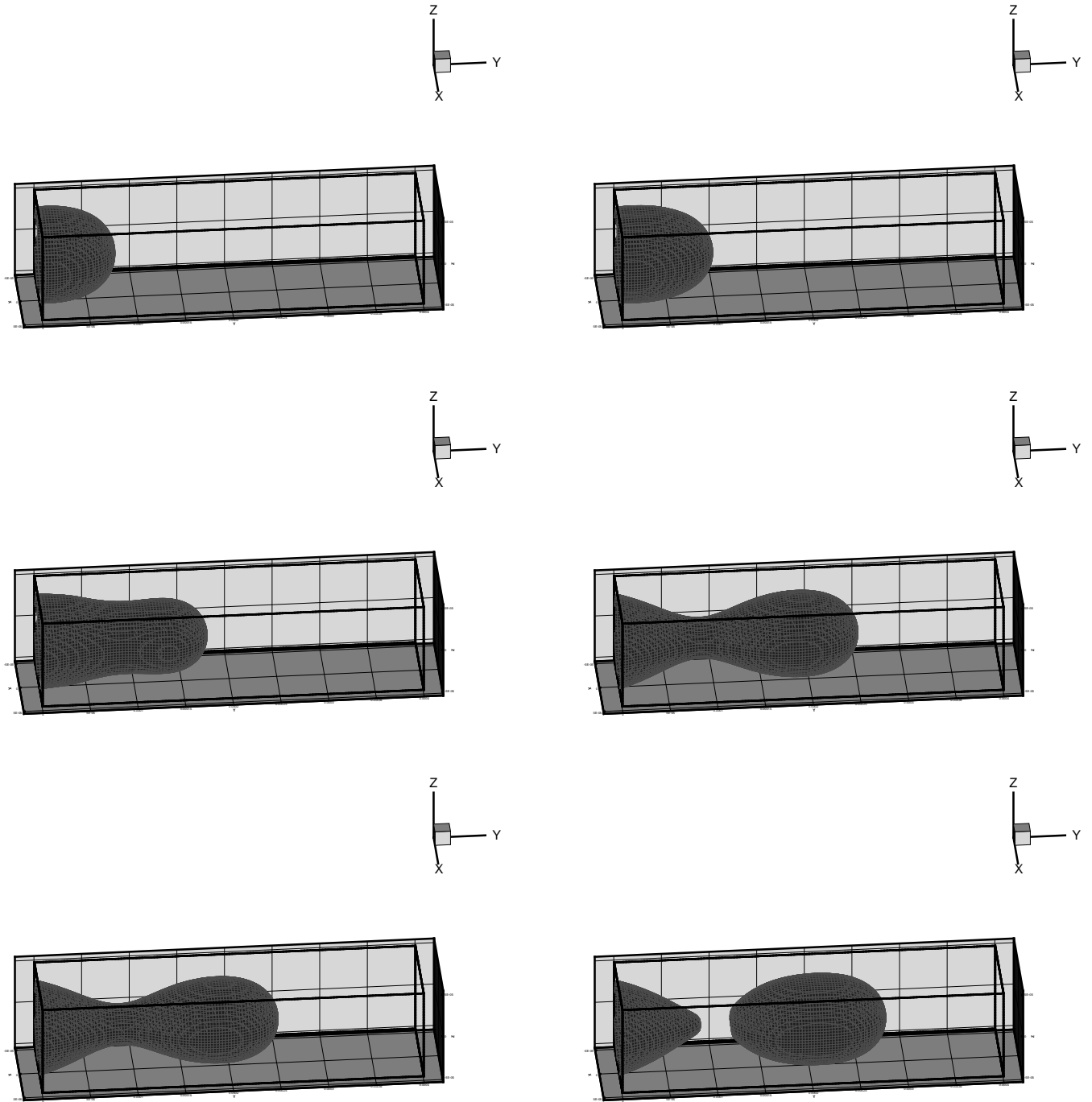


Figure 12: A sequence of figures showing the development and detachment of an air bubble in the crossflow mixing channel. Flow rates correspond to $Q_L/(Q_L + Q_G) = 0.67$.

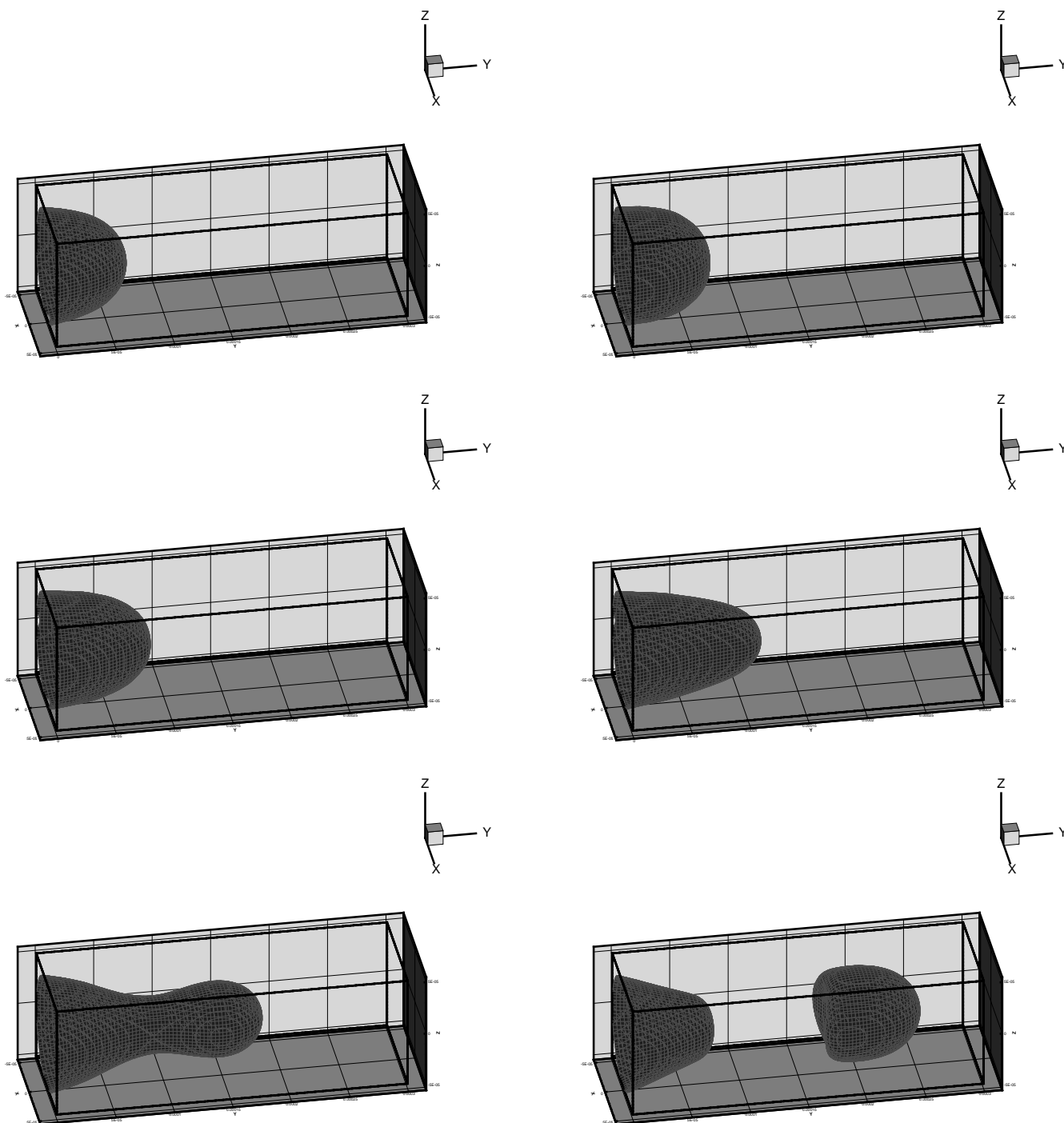


Figure 13: A sequence of figures showing the development and detachment of an air bubble in the crossflow mixing channel. Flow rates correspond to $Q_L/(Q_L + Q_G) = 0.8$.

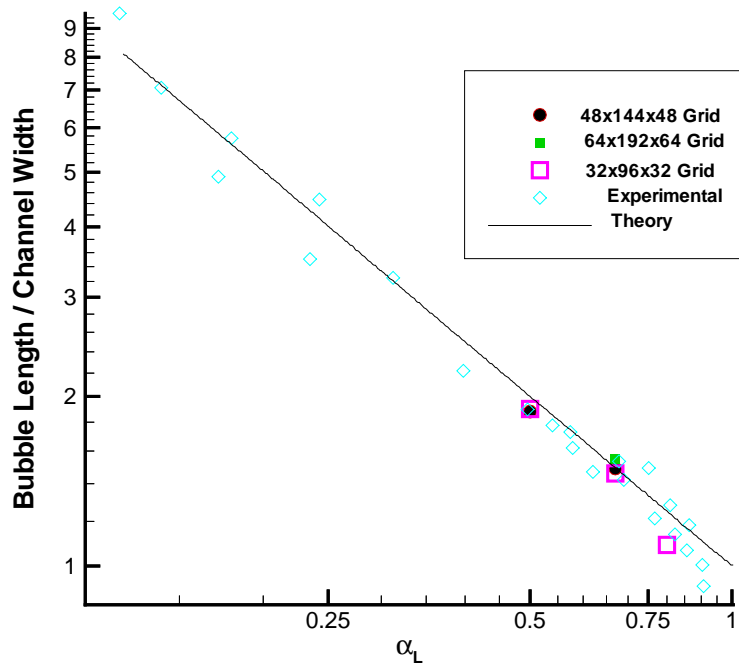


Figure 14: Comparison of numerically computed bubble sizes, for various flow rates, with experimental results of Cubaud et. al. [1] and prediction from theoretical analysis.

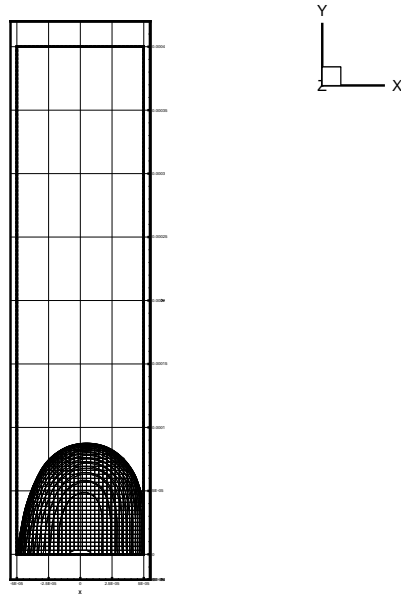


Figure 15: A section of the 3-D numerical result for T-section mixing channel flow showing the asymmetric growth of the bubble. Flow rates correspond to $Q_L/(Q_L + Q_G) = 0.5$.

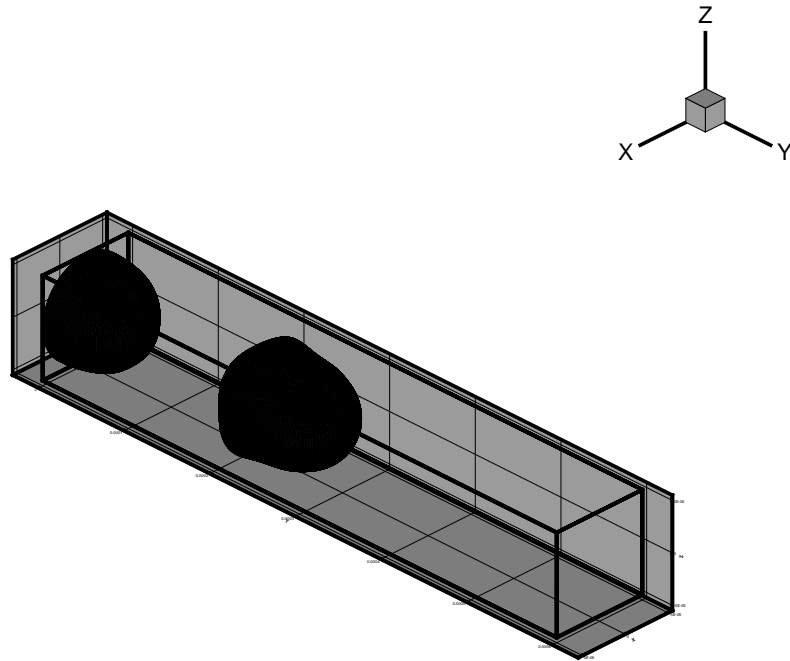


Figure 16: An instantaneous plot of the zero level set showing detachment of an air bubble in a long crossflow mixing channel. Flow rates correspond to $Q_L/(Q_L + Q_G) = 0.6$.